

DIRECT OBSERVATIONS OF THE CURRENT STRUCTURE IN THE JAPAN/EAST SEA

Shcherbina A.Y., Talley L.D.

Scripps Institute of Oceanography, La Jolla, USA

Introduction

Direct velocity measurements from the two cruises, completed in the summer of 1999 by R/Vs “Revelle” and “Khromov”, covering the whole Japan/East Sea (Fig. 1) were investigated.

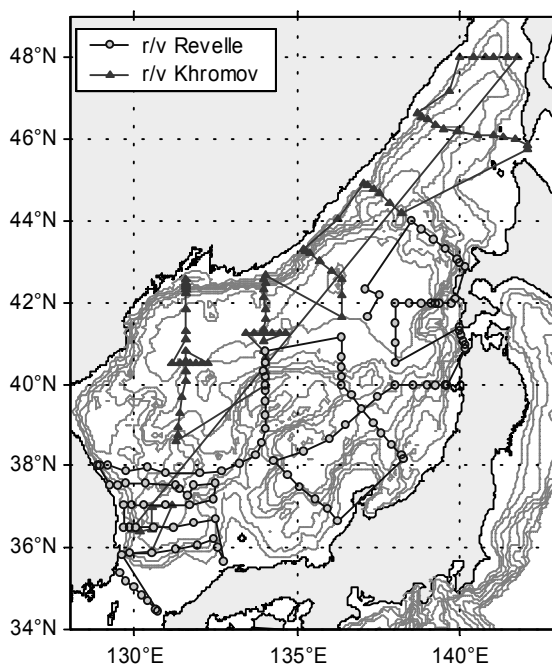


Fig. 1. Station positions

The following methods of velocity measurement were used and compared in this study:

- 1) lowered acoustic Doppler current profiler (LADCP). A self-contained broadband 150 kHz RDI ADCP was mounted on a standard Rosette frame to provide top-to-bottom velocity profile with each CTD cast. Raw velocity data were processed to utilize CTD and navigation information. The instrument and the processing software were provided by P. Hacker and E. Firing (University of Hawaii);
- 2) shipboard acoustic Doppler current profiler (ADCP) provided velocity information in the upper 300 m with five minute sampling interval. This data source was available only for the first part of the survey. Data were processed using the Common Oceanographic Data Access System (CODAS) software package;
- 3) geostrophic velocity calculations based on CTD data were used for consistency check and large-scale background estimate.

LADCP Performance

The first use of LADCP was reported by Firing & Gordon (1990), and the issue of the performance of the instrument is still under investigation. In this study, LADCP accuracy was tested by comparison with shipboard ADCP over the common depth range. The mean differences between LADCP velocity and time-average of ADCP profiles over a cast are shown in Fig. 2. It can be seen that LADCP performance strongly depends on the total depth of the station. For stations deeper than 500 m the mean error is of order of 2-3 cm/s, which is close to theoretical predictions (Firing & Gordon, 1990). The largest errors

occur when a significant portion of a profile is missing due to bottom interference or excessive package tilt, both conditions being common on shallow stations with strong currents.

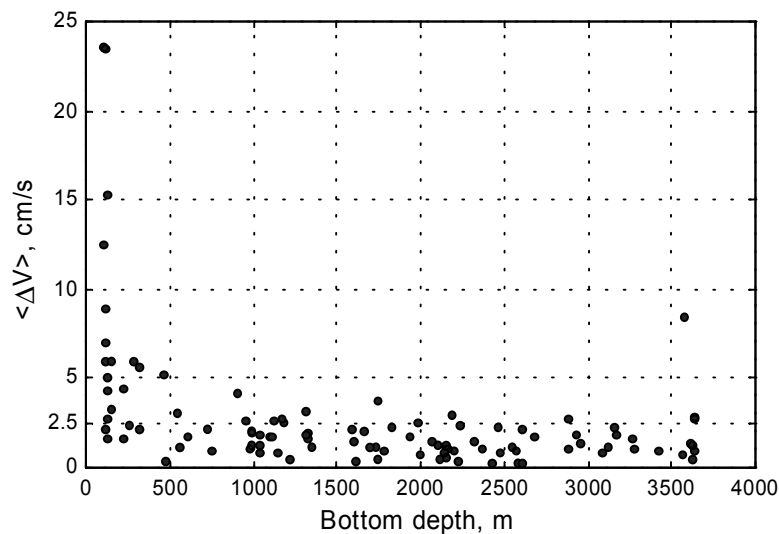


Fig. 2. LADCP error (compared to ADCP)

Other sources of inaccuracy apparently include GPS and gyrocompass errors, as well as the intrinsic profiler errors. Final absolute LADCP velocity is the result of integration of vertical shear, measured over the cast, corrected for the ship drift. Therefore, most of the error accumulates in the low vertical wavenumbers – barotropic and first baroclinic modes.

It should be noted that ADCP data were available only for the first part of the survey, and the LADCP error cannot be estimated for the second part, completed by a different ship. The latter part was characterized by quite strong ship drift that led to various degrees of data loss due to the package tilt on about 10% of the stations. Except for those stations, over-all error was presumably consistent with the above estimate.

Subpolar Front

Special attention was dedicated to the subpolar front, spanning the Japan/East sea at about 40°N. Two front crossings along 134°E were performed within the two-month period. Fig. 3 shows the contours of dynamic height in the frontal zone, based on the whole CTD dataset. The large-scale current structure of the front was distorted by a large anticyclonic eddy, located to the southeast of the section.

Also shown in Fig. 3 is the location of first cross-frontal section, occupied on June 2-4, 1999. During the second front crossing (August 6, 1999), part of the section north of 40°N was repeated.

The baroclinic structure of the subpolar front was dominated by downward-propagating near-inertial waves. Fig. 5 shows a characteristic LADCP profile taken on July 3, the day following a strong wind event with wind speed reaching 15 m/s (Fig. 4). The left panel shows the hodograph of current speed, and vertical profiles of velocity components are given in the right panel. An internal wave with velocity amplitude over 10 cm/s was observed in the upper 250 m. The velocity vector turns clockwise with depth, which means that the group velocity and energy flux are downward (Leaman & Sanford, 1975).

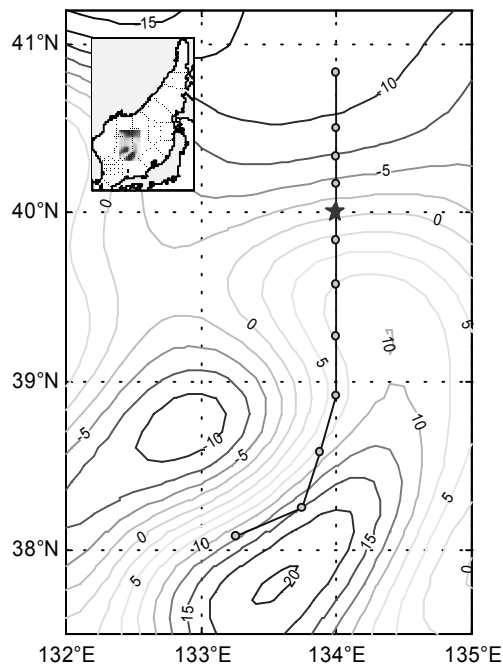


Fig. 3. Dynamic height contours (relative to 440 m, cm) in the frontal zone. Also shown is the location of the first cross-frontal section

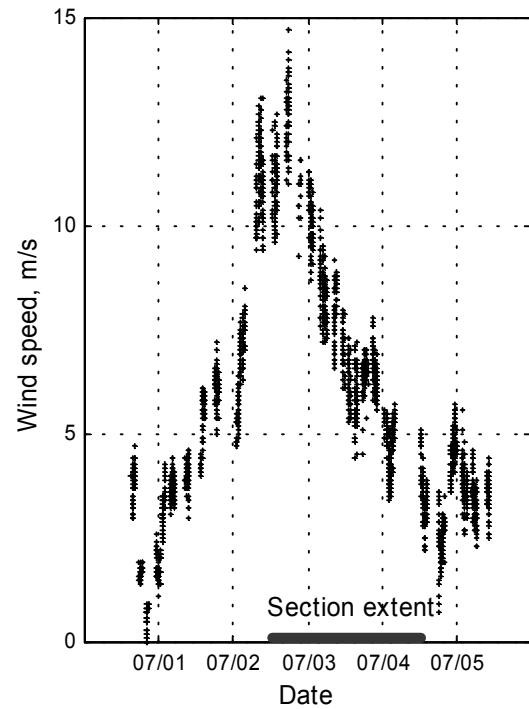


Fig. 4. On-station wind speed

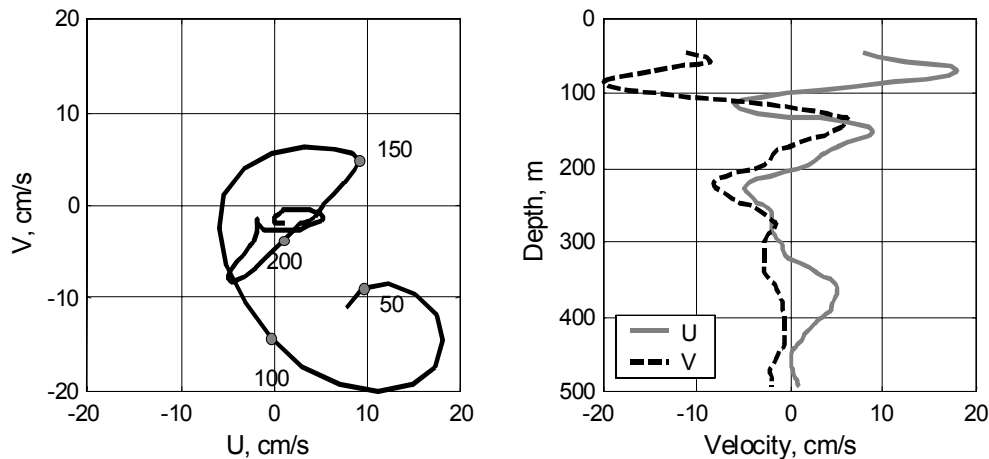


Fig. 5. Velocity hodograph, with numbers indicating depth (left). Component profiles (right). Station position (40°N , 134°E) is marked by star in Fig. 3

The spatial structure of this particularly strong internal wave was studied using the shipboard ADCP. Fig. 6 shows the cross-frontal section of vertical shear with the contours of cross-section geostrophic velocities overlain. The subpolar front is visible as a pair of closely spaced eastward-flowing jets with a maximum speed of about 30 cm/s. An internal wave packet with the group velocity directed obliquely southward and down appears to be trapped at the warm (south) side of the front (39.3°N - 40°N). Trapping and amplification of near-inertial waves in the regions of negative relative vorticity has been observed and modeled by Kunze (1984, 1985) and Wang (1991), and our results are quite consistent with those studies. Another example of near-inertial wave trapping is associated with the periphery of the anticyclonic eddy situated to the southeast of the section (38.3°N - 39°N). Because of inadequate sampling, it was impossible to investigate the vorticity structure of the eddy as well as its correlation with the wave trapping.

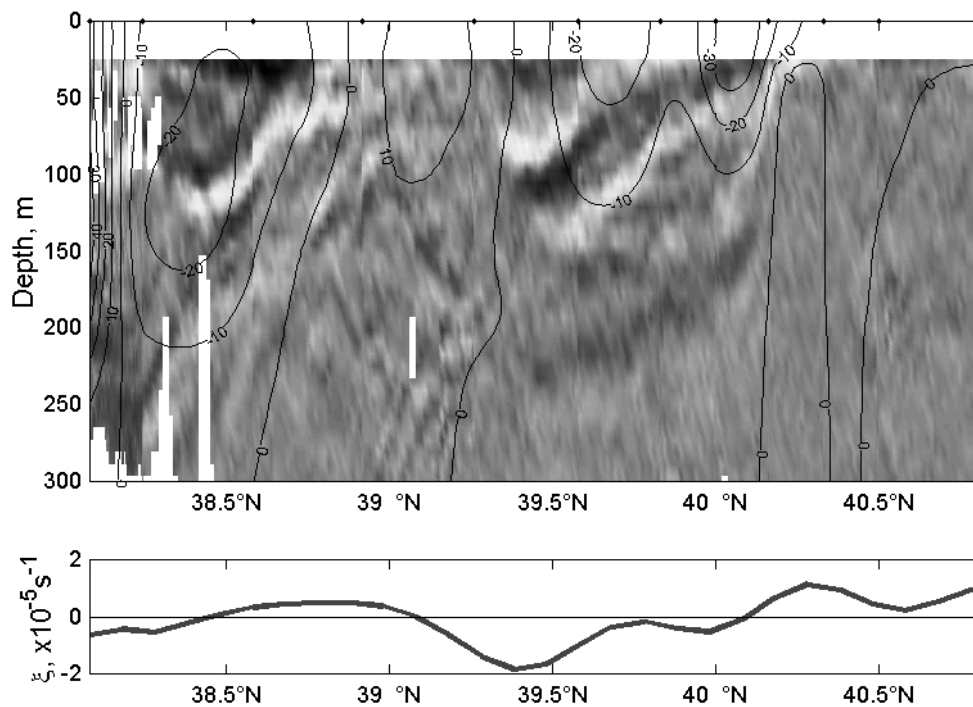


Fig. 6. Vertical shear, -measured by ADCP on the first cross-frontal section. Contours show the cross-section geostrophic velocity. Geostrophic relative vorticity is shown in the lower panel

Rotary Spectrum Studies

The rotary spectrum (in vertical wavenumbers) of ADCP shear in the frontal zone (Fig. 7) shows the predominance of clockwise-with-depth polarized internal waves by an order of magnitude. This separation corresponds to net downward energy flux, that is characteristic of wind-generated internal waves. Clockwise spectrum peaks at vertical wavelength of about 75 m. The horizontal wavelength, inferred from the slope of the crests is about 50 km. Such a large difference between the vertical and horizontal wavelengths is, in fact, the only available evidence of near-inertial character of the observed internal waves.

The cross-frontal section of integrals of clockwise and counterclockwise parts of rotary spectrum is shown in Fig. 8. The significant increase in the energy of downward-propagating waves is the evidence of near-inertial waves trapped in the regions of negative vorticity. Upward and downward propagating energies were also compared using LADCP data. Although the LADCP generally underestimates shear variance due to smoothing at high wave numbers, relative increase in the clockwise variance in the regions of negative vorticity is consistent with that shown by ADCP. Taking that into account, we can compare this section with another one, which was taken a month later by R/V “Khromov” (Fig. 9). No ADCP data were collected on that section, so comparisons have to be made between LADCP-derived shear variances.

Although winds were calmer at the time of this section, separation between clockwise and counterclockwise variances is as evident as it was on the former section. Thus, the presence of trapped near-inertial waves of significant amplitude appears to be a robust feature of the frontal zone.

Mean Energy Flux

Fig. 10 shows the dependence of the ratio of clockwise to counterclockwise shear variance (CW/CCW ratio) on the depth, averaged over the whole basin. The predominance of downward energy flux in the upper 600 m obviously corresponds to the penetration of wind energy into the upper ocean by means of clockwise-polarized near-inertial waves. A statistically significant peak in the counterclockwise shear variance at 1500 m indicates significant upward energy flux from the bottom. We believe this to be a manifestation of interaction of the mean flow with topography, resulting in internal wave radiation. The correlation of CW/CCW ratio with the topography features is under investigation.

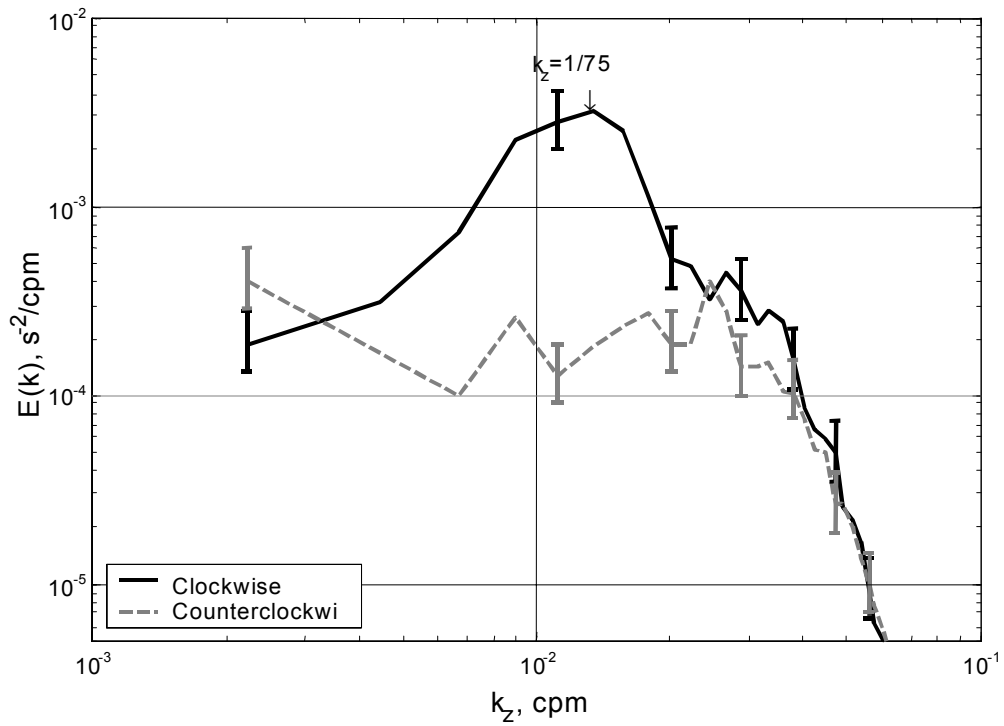


Fig. 7. ADCP shear rotary spectrum (vertical wavenumbers). 5% confidence intervals are shown

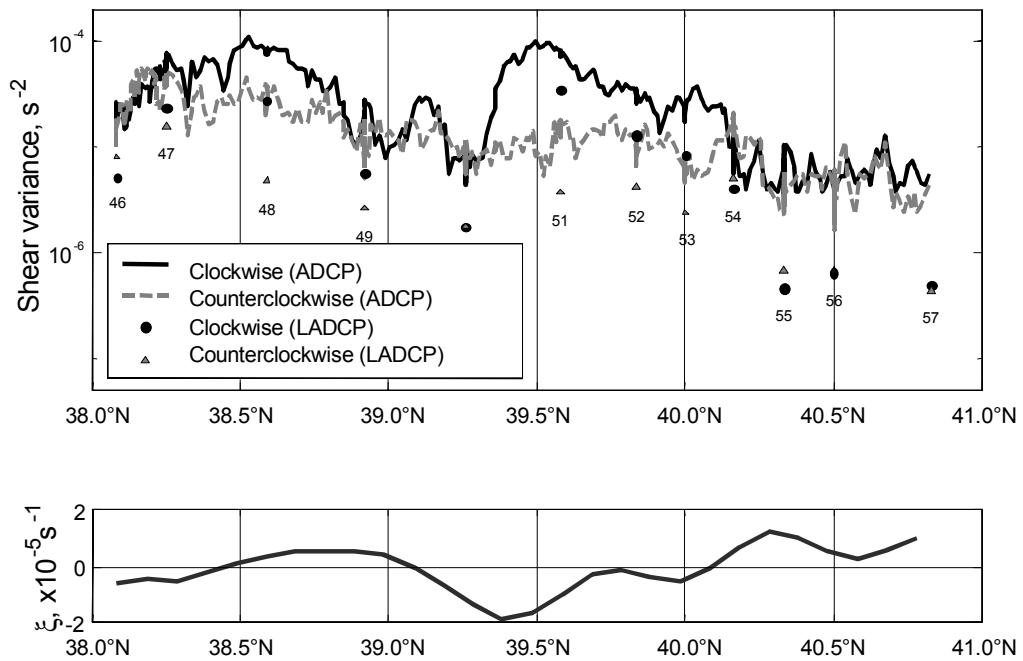


Fig. 8. Rotary shear variance (top panel) and relative vorticity (bottom panel).
June 2-4, 1999 (first front crossing)

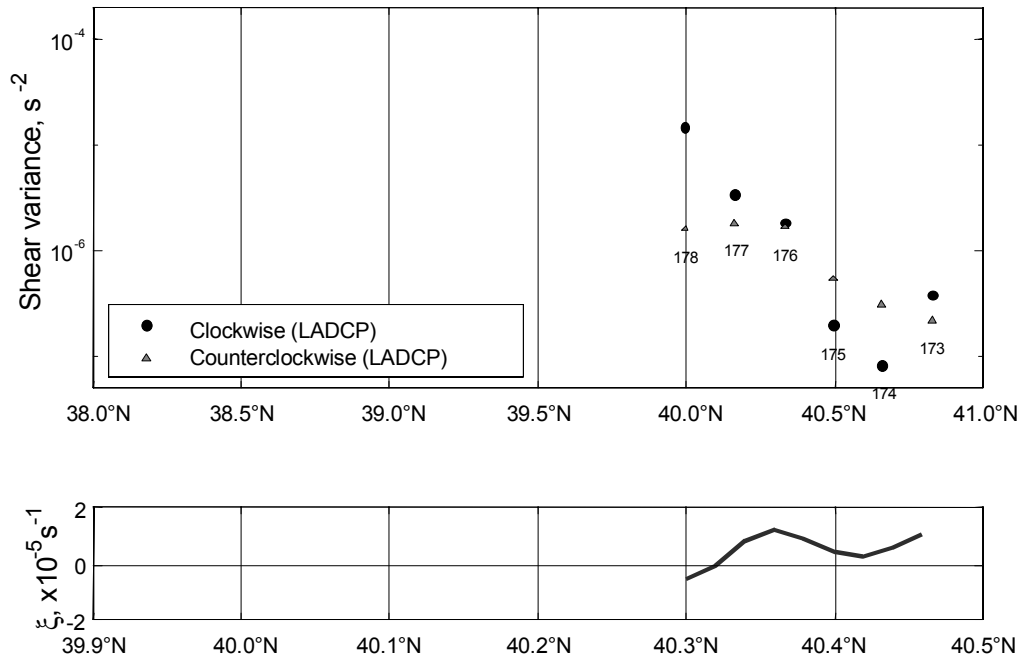


Fig. 9. Rotary shear variance (top panel) and relative vorticity (bottom panel). August 6, 1999 (second front crossing)

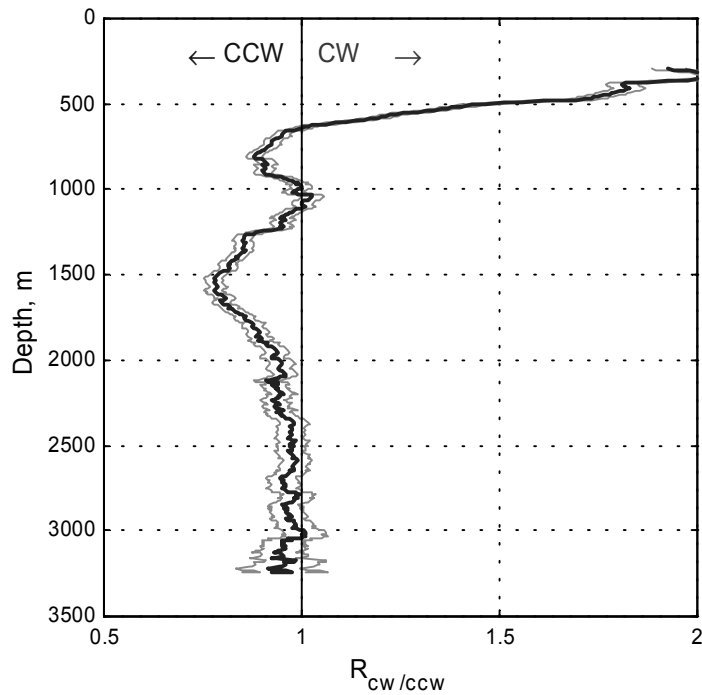


Fig. 10. Clockwise- to counterclockwise-with-depth polarization ratio. 95% confidence interval is shown

References

1. Firing E. & Gordon R. 1990. Deep acoustic Doppler current profiling // Proc. IEEE Fourth Working Conference on Current Measurements. Clinton. Maryland. P. 192-201.
2. Kunze E. & Sanford T. 1985. Observations of near-inertial waves in a front // J. Physical Oceanography. Vol. 14. P. 566-581.
3. Kunze E. 1985. Near-inertial wave propagation in geostrophic shear // J. Physical Oceanography. Vol. 15. P. 544-565.
4. Leaman K. & Sanford T. 1975. Vertical energy propagation of internal waves: a vector spectral analysis of velocity profiles // J. Geophysical Research. Vol. 80. N 15. P. 1975-1978.
5. Wang D.-P. 1991. Generation and propagation of inertial waves in the subtropical front // J. Marine Research. Vol. 49. N 4. P. 619-633.